(2)

NRL Memorandum Report 5105

Dielectronic Recombination Rates, Ionization Equilibrium, and Radiative Emission Rates for Mn Ions in Low-Density High-Temperature Plasmas

V. L. JACOBS AND J. DAVIS

Plasma Radiation Branch
Plasma Physics Division

June 23, 1983

This work was supported in part by the National Aeronautics and Space Administration and the Office of Naval Research.

NAVAL RESEARCH LABORATORY
Washington, D.C.

SECURITY CLASSIFICATION OF THIS PAGE (When Data Entered)

REPORT DOCUMENTATION PAGE		READ INSTRUCTIONS BEFORE COMPLETING FORM
1. REPORT NUMBER NRL Memorandum Report 5105	2. GOVT ACCESSION NO. AD-A129758	3. RECIPIENT'S CATALOG NUMBER
4. TITLE (and Subtitle) DIELECTRONIC RECOMBINATION RATES, IONIZATION EQUILIBRIUM, AND RADIATIVE EMISSION RATES FOR Mn IONS IN LOW-DENSITY HIGH-TEMPERATURE PLASMAS		5. TYPE OF REPORT & PERIOD COVERED Interim report on a continuing NRL problem.
		6. PERFORMING ORG. REPORT NUMBER
7. AUTHOR(s) V.L. Jacobs and J. Davis		8. CONTRACT OR GRANT NUMBER(s)
9. PERFORMING ORGANIZATION NAME AND ADDRESS Naval Research Laboratory Washington, DC 20375		10. PROGRAM ELEMENT, PROJECT, TASK AREA & WORK UNIT NUMBERS 61153N; RR011-09-41; 47-0911-0-3
11. CONTROLLING OFFICE NAME AND ADDRESS Office of Naval Research Arlington, VA 22217		12. REPORT DATE June 23, 1983
		13. NUMBER OF PAGES 20
14. MONITORING AGENCY NAME & ADDRESS(if different from Controlling Office)		15. SECURITY CLASS. (of this report) UNCLASSIFIED
		15a. DECLASSIFICATION/DOWNGRADING SCHEDULE

16. DISTRIBUTION STATEMENT (of this Report)

Approved for public release; distribution unlimited.

17. DISTRIBUTION STATEMENT (of the abstract entered in Block 20, if different from Report)

18. SUPPLEMENTARY NOTES

This work was supported in part by the National Aeronautics and Space Administration and the Office of Naval Research.

19. KEY WORDS (Continue on reverse side if necessary and identify by block number)

Recombination	High temperature
Manganese	Plasma

20. ABSTRACT (Continue on reverse side if necessary and identify by block number)

The dielectronic recombination rates for Mn ions have been calculated with account taken of the most important autoionization processes and stabilizing radiative transitions. The relative abundances of the various ionization stages have been determined using a corona equilibrium model in which electron impact ionization and autoionization following inner-shell electron excitation are balanced by direct radiative and dielectronic recombination. The power radiated by a hydrogen plasma containing Mn as an impurity has been calculated taking into account resonance line emission,

(Continues)

DD FORM 1 JAN 73 1473 EDITION OF 1 NOV 65 IS OBSOLETE
S/N 0102-014-6601

SECURITY CLASSIFICATION OF THIS PAGE (When Data Entered)

20. ABSTRACT (Continued)

direct recombination radiation, dielectronic recombination radiation, and electron — (Mn) ion bremsstrahlung. Resonance line emission is dominant at temperatures for which partially-stripped ions are abundant.

CONTENTS

DIELECTRONIC RECOMBINATION RATES, IONIZATION EQUILIBRIUM, AND RADIATIVE EMISSION RATES FOR Mn IONS IN LOW-DENSITY HIGH-TEMPERATURE PLASMAS

I. Introduction

The analysis of optically-thin far-ultraviolet and x-ray emission lines of multiply-charged ions is one of the basic methods for determining the temperatures and densities of laboratory and astrophysical plasmas. In addition, the energy balance in these plasmas can be significantly influenced by the emission of radiation from relatively low concentrations of multiply-charged atomic ions. Because the populations of the excited levels are expected to depart substantially from their local thermodynamic equilibrium values (Griem 1964), a detailed treatment of the elementary collisional and radiative processes must be employed in order to predict the emission line intensities.

In this investigation ~~we~~ the authors present the results of calculations based on a corona equilibrium model (Jacobs et al 1977, Davis et al 1977) in which a detailed evaluation is made of the dielectronic recombination rate coefficients. The ionization structure is determined by assuming that electron impact ionization and autoionization following inner-shell electron excitation from each ground state are balanced by direct radiative and dielectronic recombination. The spectral line intensities emitted by the low-lying excited states, which are assumed to undergo spontaneous radiative decay in times that are short compared with the collision time, are evaluated in terms of the corona ionization equilibrium distributions of the ground states and their electron-impact exciation states.

Manuscript approved April 11, 1983.

II. Dielectronic Recombination

Dielectronic recombination (Burgess 1964) may be described as a two-step process. First, there is a radiationless capture of a plasma electron into a $n\ell$-state accompanied by an excitation $i \rightarrow j$ of the recombining ion core $X^{+(z)}$

$$X^{+(z)}(i) + e^{-} \rightarrow X^{+(z-1)}(j, n\ell).$$

Recombination is accomplished if, instead of autoionizing, the doubly-excited state $j, n\ell$ undergoes a stabilizing radiative transition to a singly-excited state $i, n\ell$ which lies below the ionization threshold

$$X^{+(z-1)}(j, n\ell) \rightarrow X^{+(z-1)}(i, n\ell) + \hbar\omega.$$

In the corona model approximation, the initial state i is assumed to be the ground state g. The many-electron states i, j, etc. will be specified by giving the effective principal and angular momentum quantums numbers of the active electron. The influence of the spectrator electrons is taken into account in the evaluation of the transition rates.

For a Maxwellian electron electron velocity distribution the total dielectronic recombination rate coefficient is given in the corona model approximation (Shore 1969) by

$$\alpha_d(i) = 2^3 a_o^3 \pi^{3/2} (E_H/k_B T_e)^{3/2}$$

$$X \sum_{j,n\ell} \frac{g(j,n\ell)}{2g(i)} \frac{A_a(j,n\ell \rightarrow i) A_r(j,n\ell \rightarrow i,n\ell)}{A_a(j,n\ell) + A_r(j,n\ell)}$$

$$X \exp \frac{E(i) - E(j, n\ell)}{k_B T_e},$$

where the statistical weights associated with the energy levels $E(i)$ and $E(j, n\ell)$ are denoted by $g(i)$ and $g(j, n\ell)$,. respectively.

For large values of n the autoionization rates A_a $(j,n\ell \rightarrow i)$, in terms of which the radiationless capture rates have been expressed, can be obtained from the threshold values of the partial-wave electron-impact excitation cross sections σ $(i,\ell_i \rightarrow j, \ell_j)$ by means of the quantum defect theory relationship dervied by Seaton (1969). In addition, the stabilizing radiative decay rates A_r $(j, n\ell \rightarrow i, n\ell)$ can be approximated by the spontaneous emission rate A_r $(j \rightarrow i)$ for the recombining ion core. These approximations are expected to be valid for $\Delta n_i = o$ core transitions, which involve large values of n. They are uncertain for $\Delta n_i \neq o$ transitions, for which small values of n play an increasingly important role with increasing Z. The total decay rates A_a $(j, n\ell)$ and A_r $(j, n\ell)$ include the rates for all allowed autoionization and radiative decay processses. For some $\Delta n_i \neq o$ transitions, autoionization into an excited state of the recombining ion makes a large contribution to the total decay rate and gives a value of α_d which is substantially smaller than predicted by the widely used formula derived by Burgess (1965).

The dielectronic recombination rate coefficients for M_n VIII $-M_n$ XXV ions have been calculated, taking into account autoionization processes and stabilizing radiative transitions which involve a single - electron electric-dipole transition of the recombining ion core. These transitions are given in Table I. The asterisk has been used to identify transitions whose contribution to α_d is influenced by autoionization into an excited state. In Table II the total dielectronic recombination rate coefficients are presented as functions of temperature. An electron density of 10^{10} cm^{-3} was used to determine the maximum value of n. However, the

dielectronic recombination rates for the Mn ions considered in this investigation are independent of density in the low-density regions of interest.

The temperature dependence of various contributions to α_d together with the direct radiative recombination rate coefficient α_r (Jacobs et al 1977) are presented for Mn VIII and Mn XVII in Figures 1 and 2, respectively. The dashed curves correspond to single-exponential representations of the form

$$\alpha_d\ (j \rightarrow i) = A\ T_e^{-3/2} \exp\ (-T_o/T_e),$$

and the parameters A and T_o obtained for several cases are presented in Table III. We hope to employ the results of this analysis to deduce a simplified procedure for calculating α_d. The present fitting procedure gives a good representation of the peak and high-temperature behavior, but the low-temperature behavior is not well reproduced. In addition the parameter T_o does not always agree with what would be predicted from the transition energy difference.

III. Corona Ionization Equilibrium

The distribution of ions with atomic number Z among the various charge states z is determined as a function of temperature by means of the corona ionization equilibrium relationships

$$N_e N(z-1)\ S(z-1,\ g) = N_e N(z)\ \alpha(z,\ g),$$

which are solved for $1 < z < Z$ together with the condition that the sum over N(z) correspond to the total abundance N_Z. Here N(z) is the number density of ions in the charge state z, which are assumed to be

predominantly in the ground state g. N_e is the electron density. $S(z-1, g)$ is the combined rate coefficient for direct electron-impact ionization (Lotz 1967) and for autoionization following electron-impact excitation (Jordan 1969). The total recombination rate coefficient $\alpha(z,g)$ is the sum of the direct radiative recombination rate coefficient (Jacobs et al 1977) and the total dielectronic recombination rate coefficient.

The relative abundances $N(z)/N_Z$ obtained for Mn VII - Mn XXVI are presented as functions of temperature in Table IV. The relative abundances for Mn XIV - MN XXVI are shown in Figure 3. The inclusion of autoionization into excited states shifts the maximum for several of the sharply-peaked curves toward lower temperatures than would be obtained by using the formula of Burgess (1965). This effect becomes more important with increasing atomic number Z. This is a consequence of the increasing importance of the affected $\Delta n_j \neq o$ transitions of the recombining ions.

IV. Radiative Emission Rates

The power radiated per unit volume from the plasma due to electron-ion collisions may be expressed in the form

$$P_Z = N_e N_Z \left[\varepsilon_Z^{(L)} + \varepsilon_Z^{(D)} + \varepsilon_Z^{(R)} + \varepsilon_Z^{(B)} \right].$$

The coefficients ε_Z have the dimensions of power X volume and are independent of density only in the corona model approximation.

The coefficient $\varepsilon_Z^{(L)}$ describing the electron-impact excitation of resonance line radiation is given by

$$\varepsilon_Z^{(L)} = \sum_{Z-1}^{Z-1} \frac{N(Z)}{N_Z} \sum_j \Delta E\,(z,\ g \rightarrow j)\ C\,(z,\ g \rightarrow j)\ X\ B\,(z,\ j \rightarrow g),$$

where $\Delta E\ (z,\ g \rightarrow j)$ are the excitation energies $C\ (z,\ g \rightarrow j)$ are the electron impact excitation rate coefficients obtained from the distorted wave calculation (Davis et al 1976), and $B\ (z,\ j \rightarrow g)$ are the branching ratios for the radiative transitions in Table I. The corona equilibrium abudnances $N(z)\ /\ N_Z$ are given in Table IV.

Radiation is emitted during the dielectronic recombination process as satellites to the resonance lines $j \rightarrow i$. The coefficient $\varepsilon_z^{(D)}$ describing dielectronic recombination satellite radiation is obtained from equation (7) when the products $C\ (z,\ g \rightarrow j)\ B\ (z,\ j \rightarrow g)$ are replaced by the partial dielectronic recombination rate coefficients for the various stabilizing radiative transitions $j \rightarrow g$, , which are summed over the outer-electron quantum number only. The radiation emitted during the cascade decay of the outer-electron has not been included, although this radiation may represent an important energy-loss process in some cases.

The coefficients $\varepsilon_z^{(R)}$ and $\varepsilon_z^{(B)}$ describing direct recombination radiation and bremsstrahlung were estimated using expression similar to those given by Griem (1964).

The radiative energy-loss rate coefficients for electron impact excitation of resonance line radiation, dielectronic recombination radiation, direct recombination radiation, and bremsstrahlung are shown in Figure 4. The various n-shells give rise to broad maxima in the resonance line and dielectronic recombination curves. The K-shell peak is due mainly to $1s \rightarrow 2p$ transitions in the H-like and He-like ions, whereas the L-and M-shell peaks are produced predominantly by $\Delta n = o$ transitions in a large

number of adjacent ionization stages. The electron impact excitation of resonance line radiation is clearly the dominant radiative energy-loss process in the temperature region where partially stripped ions are abundant.

ACKNOWLEDGMENT

The authors would like to acknowledge the extensive efforts of Mr. R. Ernst, who prepared the atomic data and plotted the figures. This work has been supported in part by the National Aeronautics and Space Administration and the Office of Naval Research.

Table 1

Stabilizing Radiative Transitions j → i

Recombining Ion	Single-Electron Transitions
Mn XXV	2p → 1s, 3p → 1s
Mn XXIV	2p → 2 1s, 3p → 1s
Mn XXIII	2p → 2s, 3p → 2s*
Mn XXII	2p → 2s, 3p → 2s*
Mn XXI	2p → 2s, 3s → 2p, 3d → 2p*
Mn XX	2p → 2s, 3s → 2p, 3d → 2p*
Mn XIX	2p → 2s, 3s → 2p, 3d → 2p*
Mn XVIII	2p → 2s, 3s → 2p, 3d → 2p*
Mn XVII	2p → 2s, 3s → 2p, 3d → 2p*
Mn XVI	3s → 2p, 3d → 2p*
Mn XV	3p → 3s, 4p → 3s*
Mn XIV	3p → 3s, 4p → 3s*
Mn XIII	3p → 3s, 3d → 3p, 4s → 3p, 4d → 3p*
Mn XII	3p → 3s, 3d → 3p, 4s → 3p, 4d → 3p*
Mn XI	3p → 3s, 3d → 3p, 4s → 3p, 4d → 3p*
Mn X	3p → 3s, 3d → 3p, 4s → 3p, 4d → 3p*
Mn IX	3p → 3s, 3d → 3p, 4s → 3p, 4p → 3p*
Mn VIII	3d → 3p, 4s → 3p, 4d → 3p

*Affected by autoionization into an excited state

Table II

Dielectronic Recombination (cm^3 sec^{-1}) Rate Coefficients

Log_{10} Te(^{o}K)	Mn VIII	Mn IX	Mn X	Mn XI	Mn XII	Mn XIII	Mn XIV	Mn XV	Mn XVI
5.2	0.11(-09)	0.20(-09)	0.17(-09)	0.27(-09)	0.25(-09)	0.21(-09)	0.27(-09)	0.13(-09)	0.55(-20)
5.4	0.25(-09)	0.33(-09)	0.30(-09)	0.37(-09)	0.34(-09)	0.29(-09)	0.34(-09)	0.15(-09)	0.18(-16)
5.6	0.35(-09)	0.41(-09)	0.36(-09)	0.40(-09)	0.35(-09)	0.28(-09)	0.32(-09)	0.13(-09)	0.23(-14)
5.8	0.34(-09)	0.38(-09)	0.33(-09)	0.34(-09)	0.28(-09)	0.22(-09)	0.25(-09)	0.92(-10)	0.44(-13)
6.0	0.26(-09)	0.29(-09)	0.25(-09)	0.24(-09)	0.19(-09)	0.15(-09)	0.16(-09)	0.58(-10)	0.30(-12)
6.2	0.17(-09)	0.19(-09)	0.16(-09)	0.15(-09)	0.15(-09)	0.88(-10)	0.95(-09)	0.33(-10)	0.11(-11)
6.4	0.10(-09)	0.11(-09)	0.93(-10)	0.90(-10)	0.68(-10)	0.49(-10)	0.53(-10)	0.18(-10)	0.24(-11)
6.6	0.53(-10)	0.62(-10)	0.52(-10)	0.49(-10)	0.37(-10)	0.27(-10)	0.28(-10)	0.96(-11)	0.32(-11)
6.8	0.31(-10)	0.33(-10)	0.28(-10)	0.26(-10)	0.20(-10)	0.14(-10)	0.15(-10)	0.50(-11)	0.30(-11)
7.0	0.16(-10)	0.17(-10)	0.15(-10)	0.14(-10)	0.10(-10)	0.72(-11)	0.76(-11)	0.26(-11)	0.23(-11)
7.2	0.83(-11)	0.89(-11)	0.75(-11)	0.71(-11)	0.53(-11)	0.37(-11)	0.39(-11)	0.13(-11)	0.15(-11)
7.4	0.43(-11)	0.45(-11)	0.38(-11)	0.36(-11)	0.27(-11)	0.19(-11)	0.20(-11)	0.66(-11)	0.87(-11)
7.6	0.22(-11)	0.23(-11)	0.19(-11)	0.18(-11)	0.14(-11)	0.94(-12)	0.10(-11)	0.33(-12)	0.48(-12)
7.8	0.11(-11)	0.12(-11)	0.97(-12)	0.92(-12)	0.68(-12)	0.47(-12)	0.50(-12)	0.17(-12)	0.26(-12)
8.0	0.55(-12)	0.58(-12)	0.49(-12)	0.46(-12)	0.34(-12)	0.24(-12)	0.25(-12)	0.84(-13)	0.14(-12)
8.2	0.28(-12)	0.29(-12)	0.25(-12)	0.23(-12)	0.17(-12)	0.12(-12)	0.13(-12)	0.42(-13)	0.70(-13)
8.4	0.14(-12)	0.15(-12)	0.12(-12)	0.12(-12)	0.87(-13)	0.60(-13)	0.63(-13)	0.21(-13)	0.35(-13)

Table II (Cont'd)

Dielectronic Recombination (cm^3 sec^{-1}) Rate Coefficients

Log_{10} Te(^oK)	Mn XVII	Mn XVIII	Mn XIX	Mn XX	Mn XXI	Mn XXII	Mn XXIII	Mn XXIV	Mn XXV
5.2	0.19(-11)	0.43(-11)	0.11(-10)	0.14(-10)	0.10(-09)	0.28(-10)	0.14(-10)	0.00(0)	0.00(0)
5.4	0.37(-11)	0.90(-11)	0.19(-10)	[illegible](-10)	0.79(-10)	0.48(-10)	0.24(-10)	0.00(0)	0.00(0)
5.6	0.71(-11)	0.17(-10)	0.30(-10)	0.36(-10)	0.75(-10)	0.51(-10)	0.26(-10)	0.00(0)	0.00(0)
5.8	0.10(-10)	0.22(-10)	0.34(-10)	0.49(-10)	0.78(-10)	0.41(-10)	0.22(-10)	0.19(-43)	0.12(-44)
6.0	0.11(-10)	0.22(-10)	0.30(-10)	0.51(-10)	0.70(-10)	0.28(-10)	0.15(-10)	0.62(-31)	0.88(-32)
6.2	0.96(-11)	0.17(-10)	0.22(-10)	0.42(-10)	0.53(-10)	0.17(-10)	0.91(-11)	0.39(-23)	0.89(-24)
6.4	0.82(-11)	0.13(-10)	0.16(-10)	0.30(-10)	0.36(-10)	0.97(-11)	0.53(-11)	0.25(-18)	0.78(-19)
6.6	0.70(-11)	0.11(-10)	0.12(-10)	0.21(-10)	0.23(-10)	0.54(-11)	0.30(-11)	0.21(-15)	0.81(-16)
6.8	0.55(-11)	0.81(-11)	0.87(-11)	0.14(-10)	0.14(-10)	0.30(-11)	0.17(-11)	0.11(-13)	0.53(-14)
7.0	0.39(-11)	0.56(-11)	0.60(-11)	0.89(-11)	0.85(-11)	0.17(-11)	0.10(-11)	0.11(-12)	0.61(-13)
7.2	0.25(-11)	0.35(-11)	0.38(-11)	0.54(-11)	0.49(-11)	0.94(-12)	0.59(-12)	0.39(-12)	0.24(-12)
7.4	0.15(-11)	0.21(-11)	0.22(-11)	0.30(-11)	0.27(-11)	0.51(-11)	0.33(-11)	0.66(-11)	0.45(-12)
7.6	0.81(-12)	0.11(-11)	0.12(-11)	0.17(-11)	0.15(-11)	0.27(-12)	0.18(-12)	0.72(-12)	0.54(-12)
7.8	0.43(-12)	0.61(-12)	0.67(-12)	0.88(-12)	0.76(-11)	0.14(-12)	0.94(-13)	0.60(-12)	0.47(-12)
8.0	0.23(-12)	0.32(-12)	0.35(-12)	0.46(-12)	0.30(-12)	0.72(-13)	0.49(-13)	0.41(-12)	0.33(-12)
8.2	0.12(-12)	0.16(-12)	0.18(-12)	0.23(-12)	0.20(-12)	0.37(-13)	0.25(-13)	0.25(-12)	0.21(-12)
8.4	0.59(-13)	0.84(-13)	0.92(-13)	0.12(-12)	0.10(-12)	0.19(-13)	0.13(-13)	0.14(-12)	0.12(-12)

Table III

Exponential Fit Parameters for Mn

RECOMBINING ION	SINGLE-ELECTRON TRANSITION	A	T_o
Mn VIII	4s → 3p	2.42 (-11)	90.7
	4d → 3p	1.47 (-11)	128.0
	3d → 3p	4.14 (-07)	62.6
Mn XIII	3p → 3s	1.85 (-07)	36.7
	3d → 3p	7.01 (-09)	44.1
	4s → 3p	4.78 (-10)	84.6
	4d → 3p	1.40 (-10)	167.0
Mn XV	3p → 3s	6.69 (-08)	31.2
Mn XVII	3d → 2p	1.21 (-07)	59.0
	2p → 2s	3.19 (-08)	109.0
	3s → 2p	3.15 (-08)	520.0

Table IV

$\log_{10} N(z)/N_z$ for Mn Ions

$\log_{10} T_e$ (°K)	Mn VIII	Mn IX	Mn X	Mn XI	Mn XII	Mn XIII	Mn XIV	Mn XV	Mn XVI	Mn XVII	Mn XVIII	Mn XIX	Mn XX	Mn XXI	Mn XXII	Mn XXIII	Mn XXIV	Mn XXV	Mn XXVI
6.0	.656	.512	.584	.949	1.59	2.44	3.69	4.91											
6.1	1.32	.858	.579	.557	.764	1.14	1.89	2.49	2.39										
6.2	2.65	1.89	1.30	.941	.770	.740	1.05	1.11	.521	3.05									
6.3	4.97	3.95	3.08	2.42	1.91	1.52	1.45	1.05	.090	1.75	3.98								
6.4			4.97	4.03	3.22	2.52	2.10	1.21	.069	1.07	2.54	4.40							
6.5					4.47	3.47	2.76	1.63	.161	.607	1.47	2.68	4.43						
6.6						4.48	3.50	2.06	.415	.402	.768	1.43	2.60	4.09					
6.7							4.44	2.74	.926	.527	.478	.697	1.37	2.32	3.15	4.31			
6.8								3.71	1.75	1.02	.614	.456	.707	1.21	1.55	2.22	3.24		
6.9									2.96	1.94	1.23	.750	.642	.755	.693	.936	1.54		
7.0									4.67	3.39	2.40	1.64	1.21	.990	.578	.460	.703		
7.1											3.81	2.78	2.08	1.56	.846	.415	.361	3.80	
7.2												3.94	2.99	2.20	1.22	.509	.207	2.88	
7.3													3.84	2.82	1.59	.641	.132	2.18	4.88
7.4													4.64	3.39	1.96	.782	.097	1.64	3.77
7.5														3.94	2.31	.932	.089	1.21	2.87
7.6														4.47	2.66	1.10	.110	.869	2.14
7.7														5.00	3.03	1.29	.167	.620	1.55
7.8															3.43	1.53	.269	.454	1.09
7.9															3.86	1.82	.421	.367	.756
8.0															4.33	2.14	.618	.350	.516
8.1															4.83	2.50	.849	.386	.353
8.2																2.88	1.10	.456	.245
8.3																3.27	1.36	.548	.172
8.4																3.65	1.52	.662	.123
8.5																4.03	1.89	.760	.090

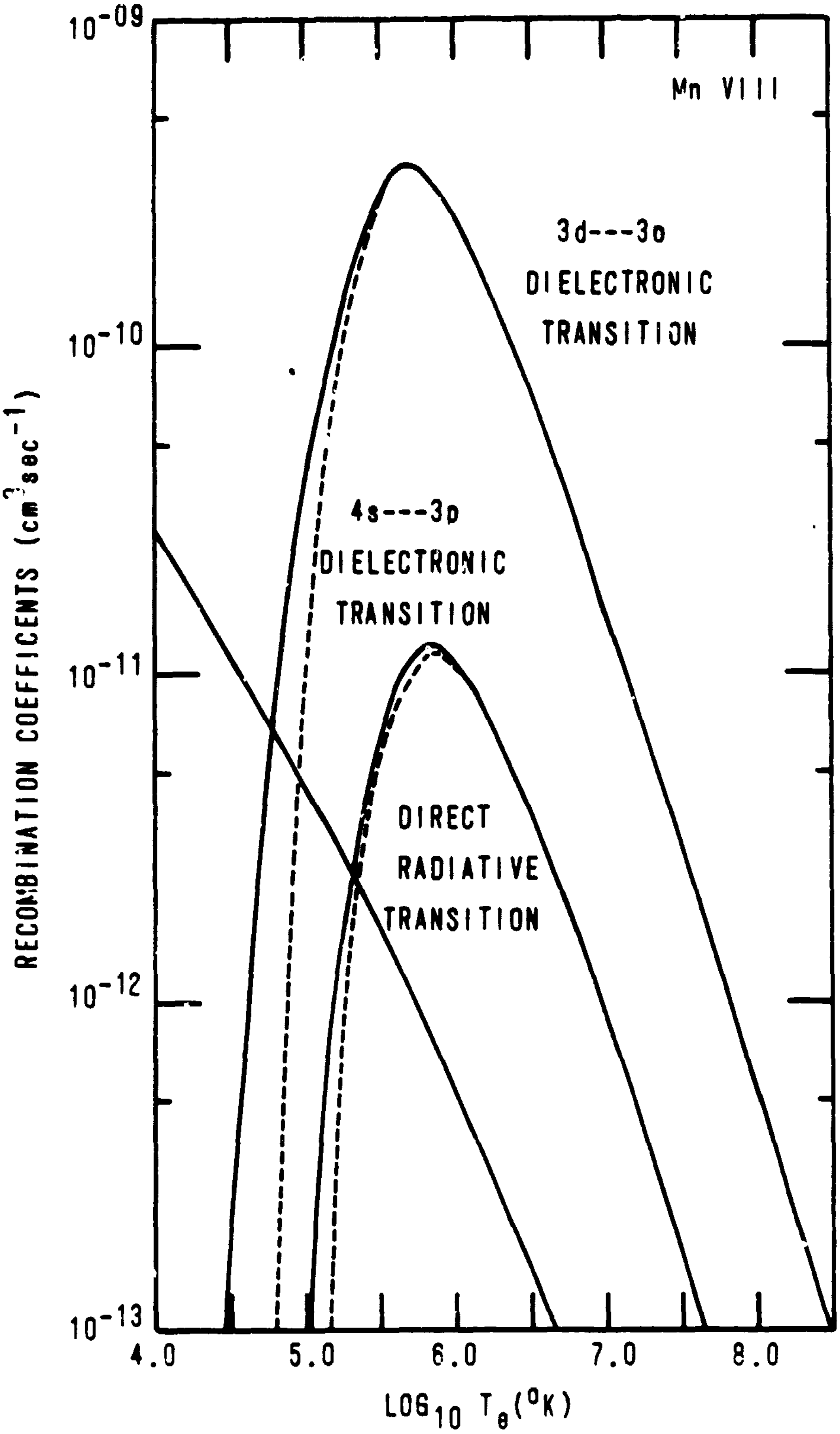

Figure 1. Direct radiative and dielectronic contributions to the Mn VIII recombination rate coefficient. Solid Curve: detailed calculation Dashed curve: single exponential fit.

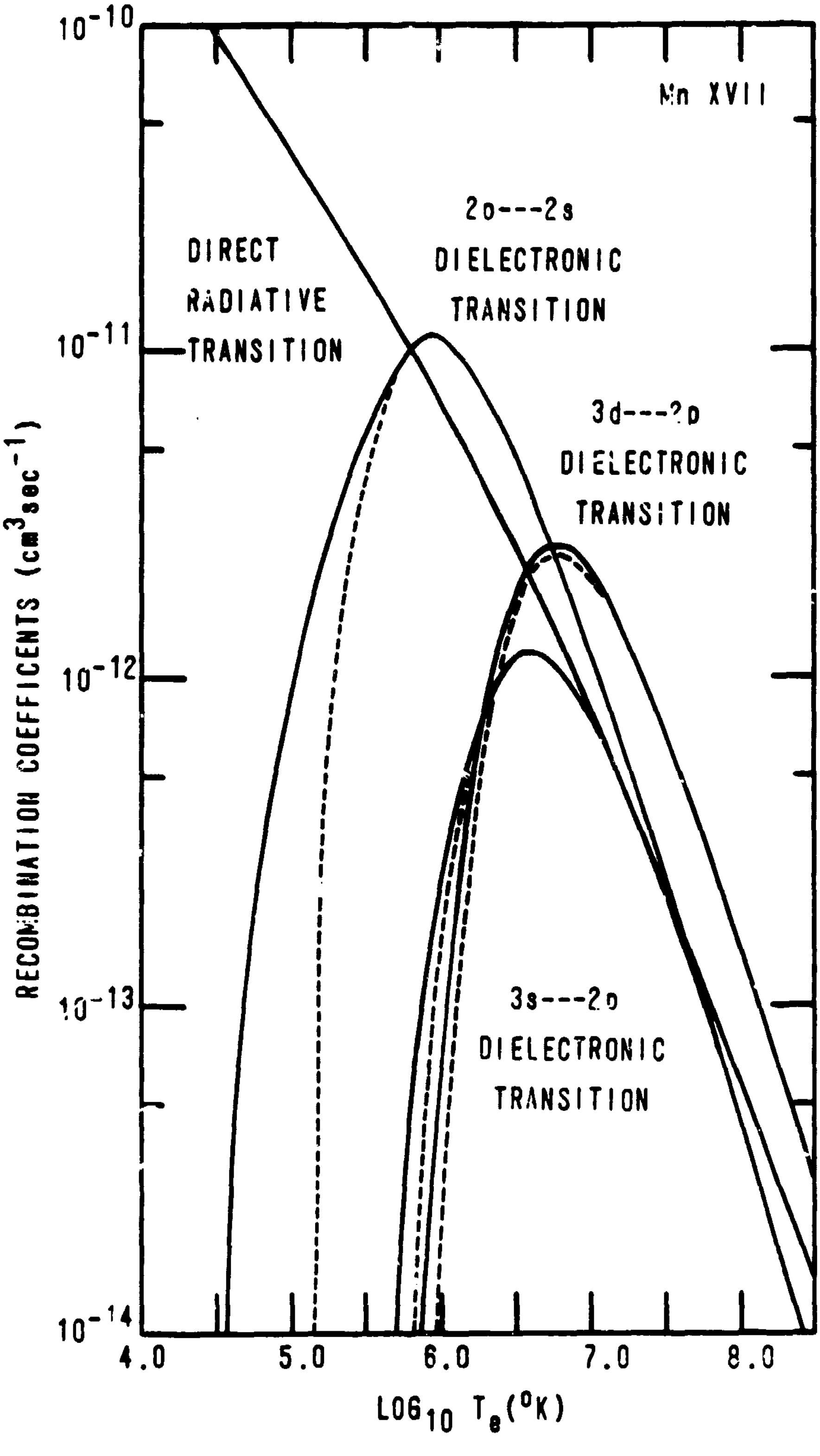

Figure 2. Direct raditive and dielectronic contributions to the Mn XVII recombination rate coefficient. Solid curve: detailed calculation dashed curve: single exponential fit.

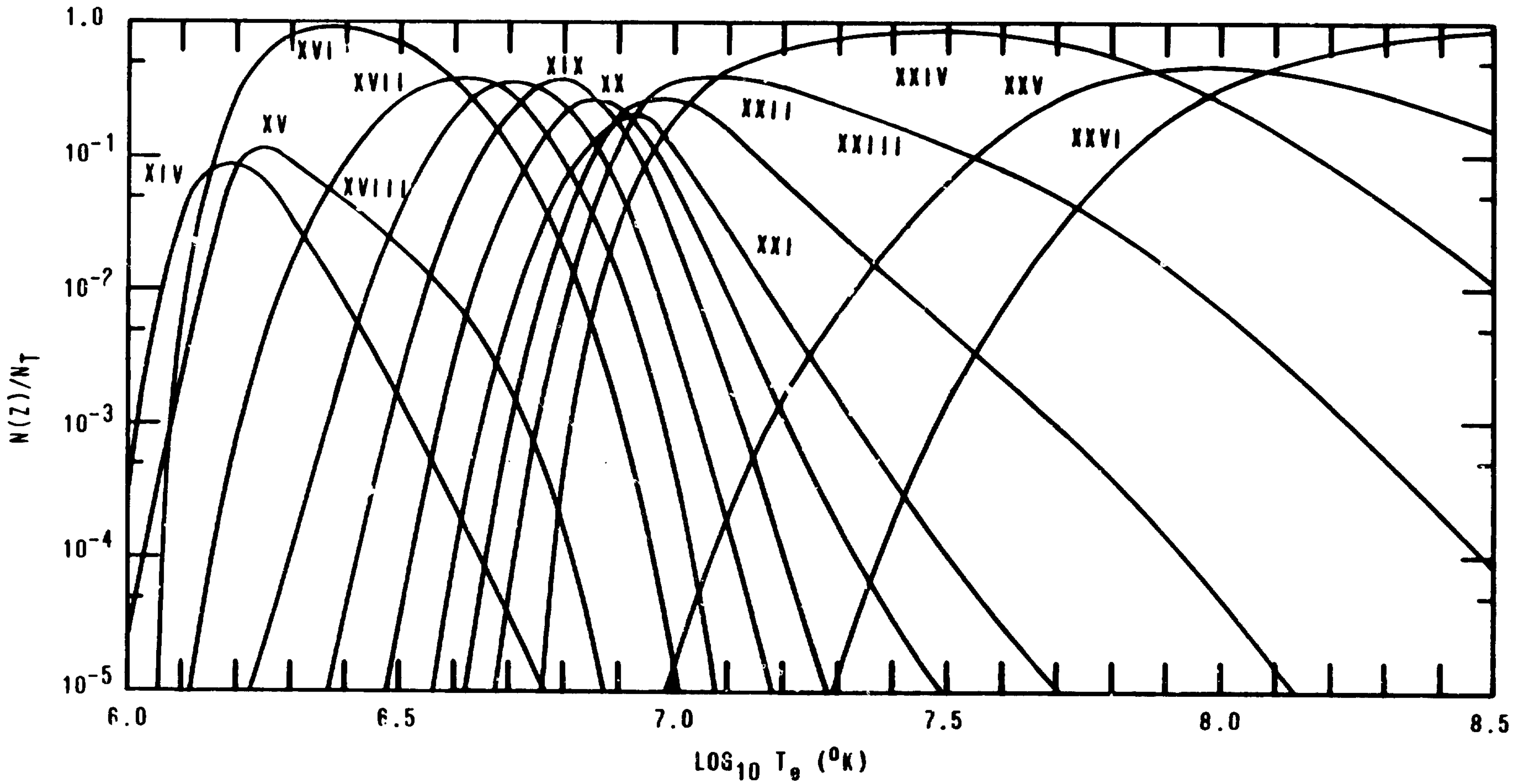

Figure 3. The corona ionization equilibrium of Mn ions.

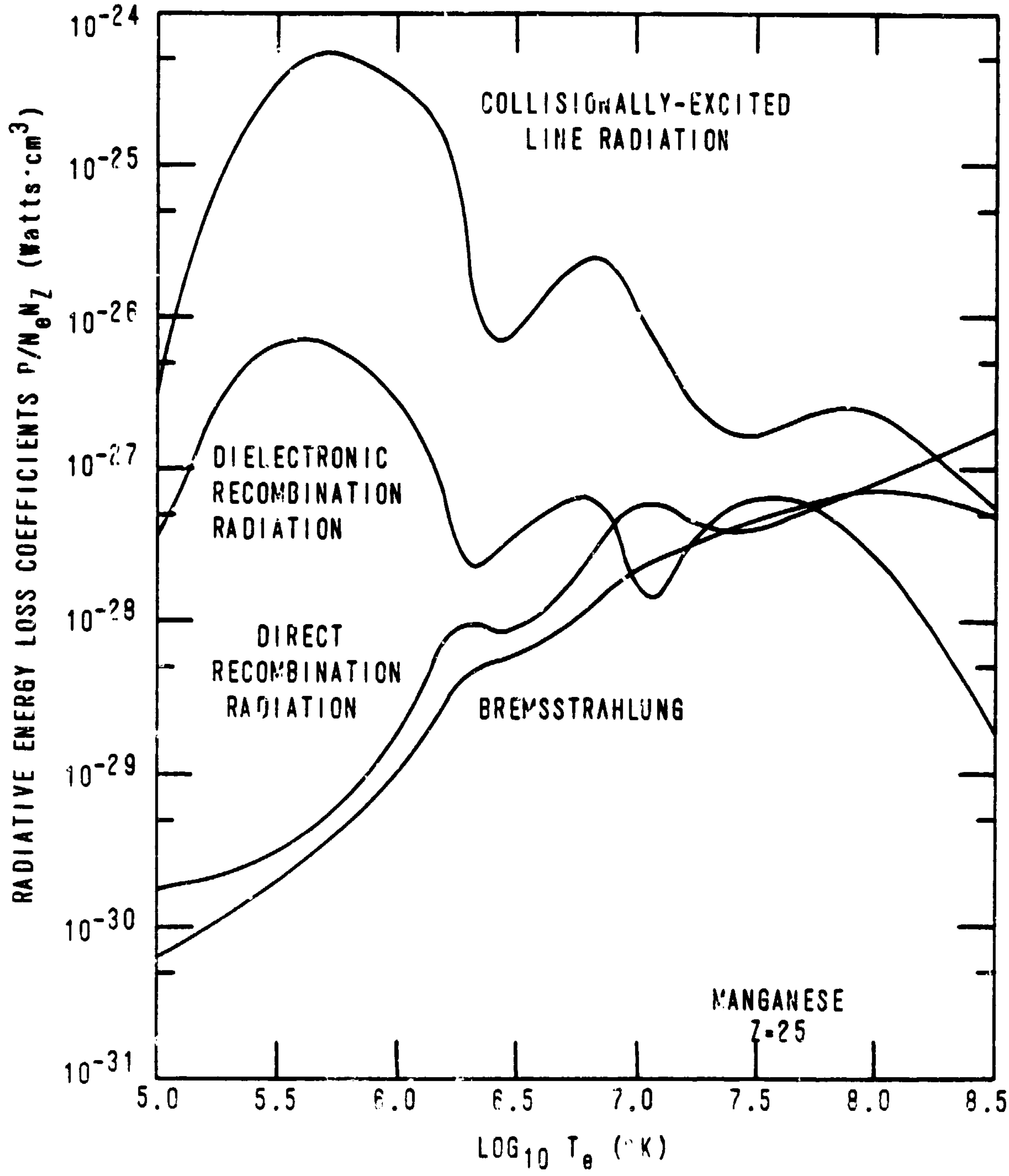

Figure 4. The radiative energy loss rate coefficients for Mn ions in corona ionization equilibrium.

References

Burgess, A. 1964, Ap. J., 134, 776.

Burgess, A. 1965, A. J., 141, 1588.

Davis, J., Jacobs, V. L., Kepple, P. C., and Blaha, M. 19 , J. Quant. Spectrosc. Rad. Transf., 17, 139.

Davis J., Kepple, P. C., and Blaha, M., 1976, J. Quant. Spectrosc. Rad. Transf., 16, 1043.

Griem, H. R., 1964 "Plasma Spectroscopy", (New York: McGraw-Hill).

Jacobs, V. L., Davis, J ., Kepple, P. C., and Blaha, M., 1977, Ap. J., 211, 605.

Jordan, C., 1969, M.N.R.A.S., 142, 501.

Lotz, W. 1967, Ap. J. Suppl., 14, 207.

Seaton, M. J., 1969, J. Phys. B, 25.

Shore, B. W., 1969 Ap. J., 158, 1205.

END

FILMED

7-83

DTIC